AIMS Materials Science, 3(2): 562-572.
DOI: 10.3934/matersci.2016.2.562
Received: 26 February 2016
Accepted: 05 May 2016
Published: 10 May 2016

http://www.aimspress.com/journal/Materials

Research article

Effect of growth time and annealing on the structural defect concentration of hydrothermally grown ZnO nanowires

Clotaire Chevalier-César [1], Martine Capochichi-Gnambodoe [1], Fang Lin [2], Dapeng Yu [2], and Yamin Leprince-Wang [1,*]

[1] Université Paris-Est, ESYCOM, UPEM, 5 bd Descartes, F-77454 Marne-la-Vallée, France
[2] State Key Laboratory for Mesoscopic Physics, Department of Physics, Peking University, Beijing 100871, China

* **Correspondence:** Email: yamin.leprince@u-pem.fr; Tel: +33-1-60957276; Fax: +33-1-60957297.

Abstract: As a low temperature and low cost synthesis method, the hydrothermal deposition is widely used to grow ZnO nanowire arrays. Their optical properties are closely related to concentration of the structural defects in the ZnO nanowires. In this work we report on investigation on the evolution of the structural defects of ZnO nanowire arrays for different growth time, before and after post-annealing. The photo-emission properties of the ZnO nanowire arrays have been investigated in detail by using photoluminescence (PL) spectroscopy both on the as-grown nanowires and on the annealed ones. The PL analysis results showed an increasing intensity in the visible emission band with the growth time which is closely related to the change of the concentration of the structural defects in the ZnO nanowires regarding to the UV near-edge emission. The visible PL emission band can be deconvoluted into three Gaussians components, which correspond to the green, yellow-orange and red emissions, respectively. It is further revealed that the intensity of the orange and red emission bands increase with the increase of the growth time, which are ascribed to the interstitial oxygen and/or hydroxide groups and adsorbed oxygen, respectively. The correlation between energy-dispersive X-ray spectroscopy (EDS) analysis and PL measurements revealed that the excess zinc can be formed in the nanowires during the hydrothermal process.

Keywords: ZnO nanowires; hydrothermal method; structural defects; photoluminescence

1. Introduction

Zinc oxide (ZnO) is a very important oxide semiconductor with great potential considering various applications, such as transparent conducting oxide (TCO) for solar cells [1,2], piezoelectricity transducers [3,4], field-effect transistors [5], chemical sensors [6–9] and light emitting devices [10–13]. Its direct wide bandgap (~ 3.37 eV) at room temperature makes the ZnO a very promising material for opto-electronic applications and its high exciton-binding energy (60 meV) allows an efficient excitonic recombination at room temperature.

ZnO nanostructures have demonstrated many interesting properties compared to the bulk material. Nowadays, ZnO nanowire arrays become the promising building blocks for various micro-/nanodevices. Many synthesis methods have been reported to obtain the ZnO nanowires, such as physical vapour deposition (PVD) [10,11], chemical vapour deposition (CVD) [14,15,16], electrochemical deposition [17,18,19] and hydrothermal method [20–23]. Although vapour deposition techniques produce high-quality well-aligned ZnO nanostructures [10], they generally require high temperature, strict elaboration conditions and expensive equipment. Mild chemical solution methods appear to be not only economical, user-friendly and ecological, but also good candidates for low-cost and large-scale industry production of ZnO nanowires. However, the fabrication of high quality hydrothermally-grown ZnO nanowires with controlled optical properties remains a crucial issue.

On the other hand, it is well known that the optical properties of the ZnO nanowires are strongly depending on their dimensionality (size) and morphology which may vary within a large extent depending on the synthesis methods and synthesis conditions, in particularly the post-annealing treatments. Li et al. synthesized ZnO nanowires both by chemical method (using $Zn(NO_3)_2$ and HMTA aqueous solution) and by thermal evaporation (from Zn oxidation in humid air; in N_2 and from ZnO/graphite, respectively), and observed three different PL spectra for three samples at different synthesis conditions [24].

In this work, the well-aligned ZnO nanowires were synthesized via the hydrothermal method on silicon substrate covered by a pre-deposited ZnO seed layer, which allows the large-area synthesis and orientation control of ZnO nanowire arrays. In order to better understand the influence of the growth time and annealing conditions on their properties, ZnO nanowires were synthesized at different growth time and annealed conditions. Two groups of ZnO nanowire samples were systematically studied by PL spectroscopy and EDS analysis.

According to the numerous reported works on this topic, the structural defect emission located in visible region in the PL spectra can be, in general, decomposed into three emissions centered at about 525 nm, 580 nm and 660 nm, respectively; corresponding to the green, yellow-orange and red emission bands, respectively. Those three emissions are usually attributed to the oxygen vacancies [25], the interstitials oxygen [24,26] and/or the hydroxides groups [27], and excess oxygen [28], respectively.

2. Materials and Method

ZnO nanowires investigated in this study were synthesized by hydrothermal method according to a previous work [29]. The Silicon substrate was well cleaned using distilled water in ultrasonic bath then in plasma cleaner. A solution of zinc acetate dihydrate ($ZnAc_2{\cdot}2H_2O$) in absolute ethanol

(0.01 M) was spun-coated onto the substrate to obtain a homogeneous thin film. The covered substrate was subsequently baked in an oven at 350 °C under atmospheric air, and a homogeneous ZnO seed layer was then formed, which acts as a nucleation layer and provides the nucleation sites for the subsequent growth of the well orientated ZnO nanowires. The nanowire growth solution was prepared by mixing equimolar aqueous solutions (0.025 M) of zinc nitrate hexahydrate ($Zn(NO_3)_2{\cdot}6H_2O$) and hexamethyltetramine (HMTA), transferred in Teflon lined autoclave. The seeded substrate was dipped into the solution at 90°C for different growth time. After the growth, the substrate covered by ZnO nanowires was withdrawn from the solution, rinsed with the distilled water and dried immediately. Samples with the growth time varied from 30 min, 1h, 3h, 4h, 5h and 6h were obtained. According to our previous work [29], the nanowire length can be tuned by the growth time, ranging from 350 nm to 1.45 μm while the diameter remained in the range of 20~40 nm. The annealing process was performed in an oven for 30 min at 400°C at ambient air.

The morphological and microstructural characterization of the ZnO nanowires have been carried out using scanning electron microscope (FEG-SEM; NEON 40 - Carl Zeiss) equipped with an energy dispersive X-ray spectrometer (EDS) for chemical element analysis. The optical properties of the ZnO nanowires were characterized via photoluminescence (PL) spectroscopy at room temperature using a micro-Raman system (RenishawInvia) and a He-Cd laser working at TEM_{00} single mode at 325 nm as excitation source. The PL measurements were carried out before and after annealing for each sample (refer to as-grown and annealed sample, respectively).

3. Results and Discussion

The amazing photoemissions of the ZnO nanocrystals have aroused great interest recently owing to its UV and visible luminescence properties at room temperature in optoelectronic device applications [28,30,31]. Figure 1 shows the PL spectra measured at room temperature for the whole series of samples with the growth time from 30 min to 6h, and the inset is the SEM picture showing the representative cross-sectional morphology of a sample grown for 6hours. For comparison, the raw spectra were first normalized with respect to the total amount of material probed. For this, normalization was done based on the morphological parameters of the nanowires (see Supplementary information). Since the penetration depth of the 325 nm laser in ZnO is less than 100 nm [32,33], the total amount of material depends mainly on the mean diameter and the density of the nanowires. The 6h sample shows a mean diameter 1.5 times larger than the rest of the series leading to 2.2 higher volume of matter. We studied the evolution of the Defect/NBE ratio with growth time, then the spectra were also normalized with respect the NBE intensity.

It is noted that the PL spectra of the as-grown ZnO nanowires show a UV emission peak at ~384 nm and a dominant and broad emission in the visible region ranging from green to red. The UV emission is well understood as near-band-edge emission, while the visible emissions are ascribed to the defect emission in the ZnO, is still not fully elucidated. Many suggestions of defects were proposed to explain the different origins, such as surface/shallow level defects, e.g. oxygen vacancies and both oxygen and zinc interstitials [26], surface hydroxides [27] as possible contributors.

A detailed analysis of the evolution trend of PL spectra from the as-grown samples for different growth time is summarized in Figure 1. As shown in Figure 1a, it is found that the normalized PL intensity of the visible emission band increases with increasing the growth time. Furthermore, a clear red-shift of the broad emission band originated from structural defects occurs for longer growth time

(6 hour for example, which can be explained by a change in the defect concentration issued from different origins of the visible emission.

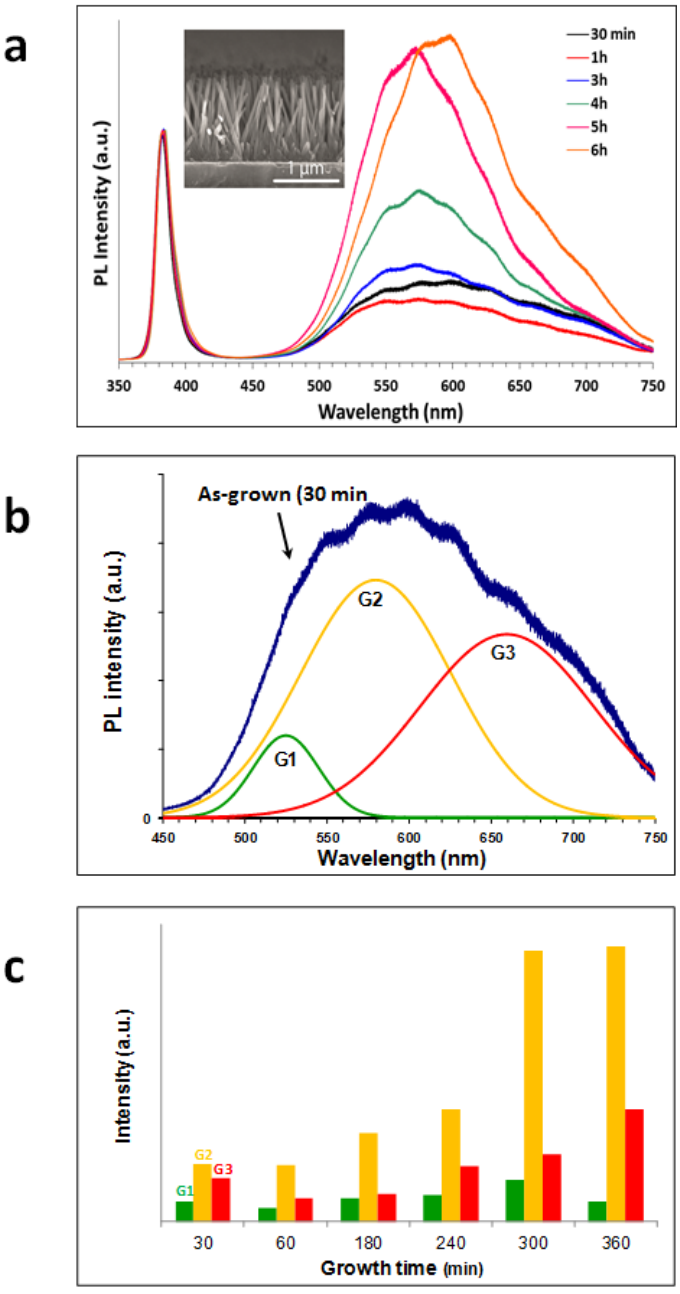

Figure 1. Analysis of the PL spectra of the as grown samples. a: PL spectra of as-grown samples as a function of the growth time. b: Visible emission band of PL spectra from a sample grown for 30min, which is fitted by 3 Gaussian components G1 (green), G2 (yellow) and G3 (red). c: Evolution with growth time of the intensity of the Gaussian components used for the fit. It is found that the normalized PL intensity of the yellow G2 component and the G3 red component increases with the increase of the growth time, while the green band remains the same.

In fact, the defect concentration inside the ZnO structure as well as on the surface of the nanowires is due to an increasing aspect ratio with the synthesis time. In literature, it has been proposed that the visible emission band is composed of three main emissions in the green (515~530 nm), the yellow-orange (570~600 nm) and the red (660~680 nm) bands, respectively [34]. This hypothesis is quite well accepted among many research groups. The green luminescence is generally associated with oxygen vacancies V_O [25]; whereas the yellow-orange emission has been assigned to interstitials oxygen (O_i) [24] and/or hydroxides groups [27,35,36] in the ZnO structure. The red emission has been reported to be associated with the oxygen excess [28,37].

For the long growth time, an apparent red-shift is observed and it may be due to an increase of the defect concentration related to the increased yellow-orange and red emissions. In fact, a long growth time could favour the formation of oxygen-rich ZnO nanowires with an increasing concentration of hydroxides groups. We would emphasize that these hydroxides could come from the precipitation of zinc hydroxide during the growth on the surface of the ZnO nanowires, but not really incorporated in the ZnO nanowire structure. Nevertheless, these defects behave like the surface defects, so they increase with the aspect ratio, thus with the growth time.

In order to make a comprehensive understanding of the PL evolution of all the samples grown for different time, the PL spectra from samples grown for different time were decomposed by using three Gaussian components, and according to references [34–37], each of the components corresponds to different origin of peculiar defects. A representative example is shown in Figure1b for the sample grown for 30 min, and the three Gaussian components are centred at ~525 nm (G1), ~580 nm (G2), and ~660 nm (G3), respectively. The G1 (green emission) correspond to the oxygen vacancy, the G2 (yellow-orange emission) is related to the interstitial oxygen, and the G3 (red-emission) originates from the oxygen from the surface. The Figure 1crepresents the intensity evolution trend of the three Gaussian components with the growth time, and it can be seen an increasing intensity of the yellow-orange (G2) and the red (G3) emissions with the growth time, suggesting an increase of the respective defect forming these emissions, i.e. interstitials oxygen (O_i)/hydroxides $Zn(OH)_x$ and adsorbed oxygen (O_{ads}), respectively. On the other hand, no significant change was observed for the green emission (G1) compared to the other two. By comparing the samples grown for 5h and 6h, we observed an evolution in the intensities related to the visible emission; the green emission was reduced and the red one increased for the sample 6h while the yellow-orange remains constant compared to the 5h, this is why we observed a red-shift in the visible emission of the PL spectrum before deconvolution for the sample 6h.

It is well known that the annealing treatment can improve crystalline quality and tune the optical properties of the ZnO nanowires [38,39]. Therefore, we have carried out an annealing treatment at 400 °C during 30 min in ambient air for all the samples of different growth time. Thus, the emissions attributed to vacancies (V_{Zn} and/or V_O) and either interstitial oxygen or hydroxide groups $Zn(OH)_x$ were expected to evolve after annealing, due to the ambient atmosphere annealing operation. The inset in Figure2a shows the cross-sectional SEM image of the annealed sample grown for 6 hours, and it can be observed that the nanowires have a similar morphology compared to the as-grown ones. In fact, for the samples with the short growth time, i.e. 30 min and 1h, the annealing treatment leads to an increase in PL intensity of the yellow-orange and red emission components due to the sorption of the oxygen during annealing. In contrast, the longer-time growth can induce the higher defect density due to the concentration variation of the solution, as is revealed in the Figure 1c. In this case, the annealing treatment suppresses mainly the green emission (resulted from the oxygen

vacancy). Furthermore, an overall red-shift of the visible emission in the PL spectra was observed compared in the PL spectra of the as-grown samples. This phenomenon is also observed by Djurišić et al. [30] for all the annealed samples (30 min @400 °C in air).

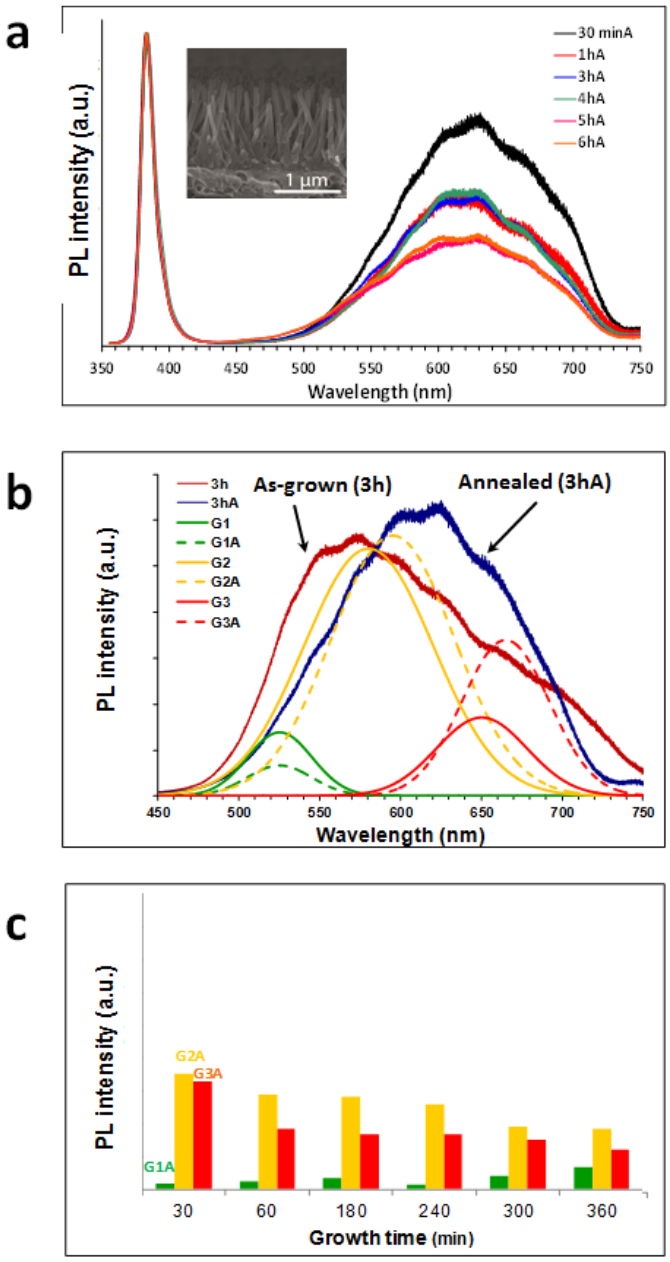

Figure 2. Analysis of the PL spectra of the annealed samples. a: PL spectra of annealed samples with different growth time. b: Visible emission band of PL spectra of as-grown (3h) sample (red) and annealed (3hA) sample (blue) and their corresponding Gaussian components (full line for as-grown and dashed line for annealed). c: Evolution of the intensity of the Gaussian components, used for the fit, with growth time after the annealing process.

The visible emission spectra of the annealed-samples were also fitted by using the same three

Gaussian components of G1A (centred at ~525 nm), G2A (~575–600 nm) and G3A (~660–680 nm) for annealed sample (dashed lines), and compared to those of as-grown samples (solid lines), and are shown in Figures 2b & 2c. From the fitted spectra, we observed a total diminishing of the green emission after annealing whereas the yellow-orange and red emissions increased for samples grown for 30 min to 3h and decreased for those grown for 4h to 6h. The annealing improved the crystal quality by diminishing the defect concentration related to the oxygen vacancies (green emission). Since the hydroxyl desorption temperature is ~150 °C [25], the emission related to this type of defects (yellow-orange) was expected to decrease after annealing. But instead of diminishing, the yellow-orange emission increased as well as the red emission for samples grown for 30 min, 1h and 3h, respectively. Then, from this observation, we supposed that the yellow-orange emission cannot be simply ascribed to hydroxides $Zn(OH)_x$ groups only; may be more than types of defects contribute to the yellow-orange emission, i.e. interstitials oxygen and hydroxide groups. The red emission also increased for these three samples, which is due to, as reported by Kwok et al. [25], the oxygen excess (O_{ads}).

From the above discussions, we can conclude that the hydrothermal process favours the formation of oxygen-rich ZnO nanowires, thus the oxygen content in long-growth-time ZnO nanowires is higher than that contained in the ambient air. As the result, excess oxygen will come out of the samples to keep a balance, and the oxygen concentration will decrease after annealing (Figure2c).

In order to follow the evolution of each element with growth time, systematic EDS analysis was performed on all samples before and after annealing. The Figure3 summarizes the Zn/O atomic ratio extracted from EDS element analysis results, which can provide a qualitative indication of the element change in the nanowires as a function of growth and annealing time. For the as-grown samples, the Zn/O ratio is smaller than the unity 1 for the 30 min to 5 hours grown samples, revealing that the total oxygen content is higher than the Zn in the samples. The adsorbed excess oxygen forms and hydroxides can contribute to raise the content of oxygen detected by EDS. Moreover, the hydrothermal synthesis takes place in the oxygen-rich milieu and the measured value of Zn/O ratio is in agreement with the formation of oxygen-rich samples. It is clear from the Figure 3 that the longer is the growth time, the higher is the EDS ratio, implying that either the oxygen content decreases, and/or the zinc concentration increases in the samples with the increase of the growth time. But the PL results (Figure 1c) showed increasing emissions related to oxygen defects (O_i, O_{ads}, hydroxydes) with growth time. From these observations, a faster increase of the zinc content compared to the oxygen could correlate both PL and EDS results. Indeed, a more important formation of zinc than oxygen would lead to increasing ratio Zn/O from the EDS analysis and the evolution of the visible PL emission attributed to the oxygen defects (O_i, O_{ads} and hydroxydes $Zn(OH)_x$). This could be explained by the formation of excess zinc in the samples as zinc interstitials, hydroxides $Zn(OH)_x$. The hypothesis of $Zn(OH)_x$ implication is consistent with the increasing of the yellow-orange emission observed in PL spectra on Figure1c. But the formation of $Zn(OH)_x$ is valid only for $x \leq 1$ otherwise the oxygen content would increase as much as zinc content. Other zinc compounds may be also responsible but it is not possible to clearly identify them here. After annealing, there are also two trends observed from EDS analysis (Figure3): the Zn/O ratio decreased for samples 30 min to 3h and increased for 4h to 6h. This evolution is in agreement with the results obtained from PL measurements, the increase of defects related to global excess oxygen (O_i, O_{ads} and hydroxydes) for samples 30minA to 3hA result in more intensive visible PL emissions

(yellow-orange and red) and then lower Zn/O EDS ratio. On the contrary, for the samples 4hA to 6hA, the diminution of oxygen content after annealing leads these PL emissions to lower and increases the Zn/O ratio, as observed by EDS. It is noteworthy that for samples 5hA and 6hA, the Zn/O ratio is over the unity which confirms the hypothesis of the excess zinc formation for longer growth time samples.

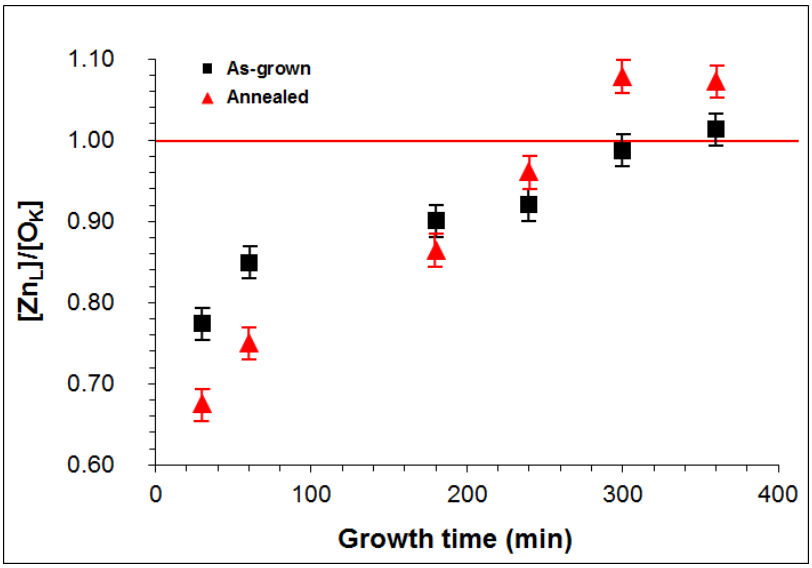

Figure 3. Zn/O compositional ratio obtained from EDS analysis both for as-grown and annealed samples.

From the PL and EDS results we have seen that the hydrothermal method promotes the formation of oxygen–rich ZnO nanowires (O_i, O_{ads} and $Zn(OH)_x$), owing to the synthesis conditions; while the annealing process improves sample quality by decomposing zinc hydroxides and reducing structural defects such as oxygen vacancies.

4. Conclusion

Aligned ZnO nanowires under different growth time were synthesized by hydrothermal method on silicon substrate using a seed layer. The optical properties of the samples were systematically studied by PL investigation and EDS analysis before and after annealing in ambient air. It was found that the normalized intensity of the PL visible emission band increases with the growth time, indicating a clear increase in the structural defect concentration. The decomposition of the observed visible PL emission band using a Gaussian components further revealed that such a PL intensity increase arises from an increased yellow-orange and red emissions with increase of the growth time, which are in turn attributed to increase of the interstitials oxygen and/or hydroxide groups and adsorbed oxygen. EDS analysis provides more evidence that the formation of excess zinc may originate from the zinc hydroxides or interstitials. The PL measurements from the annealed samples showed that the annealing process will suppress the green emission intensity related to oxygen vacancies for all samples; and influence the yellow-orange and red emissions related to the total oxygen content, depending on the growth time. The EDS analysis is in well agreement with the PL

measurements and both results confirm that the higher increase of Zn content than oxygen during growth process suggesting the formation of excess zinc for long-growth-time samples.

Conflict of Interest

The author declares no conflicts of interest in this paper.

References

1. Law M, Greene LE, Johnson JC, et al. (2005) Nanowire dye-sensitized solar cells. *Nat Mater* 4: 455–459.
2. Schlur L, Carton A, Lévêque P, et al. (2013) Optimization of a new ZnO nanorods hydrothermal synthesis method for solid state dye sensitized solar cells applications. *J Phys Chem* 117: 2993–3001.
3. Wang ZL (2011) Nanogenerators for self-powered devices and systems, Atlanta, USA.
4. Zhao MH, Wang ZL, Mao SX (2004) Piezoelectric characterization of individual zinc oxide nanobelt probed by piezoresponse force microscope. *Nano Lett* 4: 587–590.
5. Fan Z, Lu JG (2004) ZnO nanowire field effect transistor and oxygen sensing property. *Appl Phys Lett* 85: 5923–5925.
6. Liao L, Lu HB, Li JC, et al. (2007) Size dependence of gas sensitivity of ZnO nanorods. *J Phys Chem C* 111: 1900–1903.
7. Cao Y, Hu P, Pan W, et al. (2008) Methanal and xylene sensors based on ZnO nanoparticles and nanorods prepared by room temperature solid state chemical reaction. *Sensor Actuat B* 134: 462–466.
8. Al-Hilli SM, Willander M, Öst A, et al. (2007) ZnO nanorods as an intracellular sensor for pH measurements. *J Appl Phys* 102: 084304.
9. Kim JY, Jo SY, Sun GJ, et al. (2014) Tailoring the surface area of ZnO nanorods for improved performance glucose sensors. *Sensor Actuat B* 192: 216–220.
10. Huang MH, Mao S, Feick H, et al. (2001) Room temperature ultraviolet nanolasers. *Science* 292: 18971899.
11. Kong YC, Yu DP, Zhang B, et al. (2001) Ultraviolet-emitting ZnO nanowires synthesized by physical vapor deposition approach. *Appl Phys Lett* 78: 407–409.
12. Zhang XM, Lu MY, Zhang Y, et al. (2009) Fabrication of high-brightness blue-light-emitting diode using a ZnO-nanowire array grown on p-GaN thin film. *Adv Mater* 21: 2767–2770.
13. Willander M, Nur O, Zhao QX, et al. (2009) Zinc oxide nanorod based photonic devices: recent progress in growth, light emitting diodes and lasers. *Nanotechnology* 20: 332001.
14. Wang X, Summers CJ, Wang ZL (2004) Large-scale hexagonal-patterned growth of aligned ZnO nanorods for nano-optoelectronics and nanosensors arrays. *Nano Letters* 4: 423–426.
15. Gao PX, Wang ZL (2004) Substrate atomic-termination induced anisotropic growth of ZnO nanowires/nanorods by the VLS process. *J Phys Chem B* 108: 7534–7537.
16. Aad R, Simic V, Le Cunff L, et al. (2013) ZnO nanowires as effective luminescent sensing materials for nitroaromatic derivatives. *Nanoscale* 5: 9176–9180.
17. Peulon S, Lincot D (1996) Cathodic electrodeposition from aqueous solution of dense or open-structured zinc oxide films. *Adv Mater* 8: 166–170.

18. Leprince-Wang L, Yacoubi-Ouslim A, Wang GY (2005) Structure study of electrodeposited ZnO nanowires. *Microelec Journ* 36: 625–628.
19. Öztürk S, Tasaltın N, Kılınç N, et al. (2010) Fabrication of ZnO nanowires at room temperature by cathodically induced sol-gel method. *Appl Phys A* 99: 73–78.
20. Greene LE, Law M, Goldberger J, et al. (2003) Low temperature wafer scale production of ZnO nanowire array. *Angew Chem* 43: 3031–3134.
21. Vayssieres L (2003) Growth of arrayed nanorods and nanowires of ZnO from aqueous solutions. *Adv Mater* 15: 464–466.
22. Guo M, Diao P, Cai S (2005) hydrothermal growth of well aligned ZnO nanorods array: dependence of morphology and alignment ordering upon preparing conditions. *J Solid State Chem* 178: 1864–1873.
23. Yi SH, Choi SK, Jang JM, et al. (2007) Low temperature growth of ZnO nanorods by chemical bath deposition. *J Colloid Interf Sci* 313: 705–710.
24. Li D, Leung YH, Djurišić AB, et al. (2004) Different origins of visible luminescence in ZnO nanostructures fabricated by the chemical and evaporation methods. *Appl Phys Lett* 85: 1601–1603.
25. Kwok WM, Djurišić AB, Leung YH, et al. (2006) Influence of annealing on stimulated emission in ZnO nanorods. *Appl Phys Lett* 89: 183112.
26. Heo YW, Norton DP, Pearton SJ (2005) Origin of green luminescence in ZnO thin film grown by molecular beam epitaxy. *J Appl Phys* 98: 073502.
27. Xie R, Sekiguchi T, Ishigaki T, et al. (2006) Enhancement and patterning of ultraviolet emission in ZnO with electron beam. *Appl Phys Lett* 88: 134103.
28. Djurišić AB, Leung YH, Tam KH, et al. (2006) Green; yellow and orange defect emission from ZnO nanostructures: Influence of the excitation wavelength. *Appl Phys Lett* 88: 103107.
29. Chevalier-César C, Capochichi-Gnambodoe M, Leprince-Wang Y (2014) Growth mechnanism studies of ZnO nanowire arrays via hydrothermal method. *Appl Phys A* 115: 953–960.
30. Djurišić AB, Leung YH, Tam KH, et al. (2007) Defect emission in ZnO. *Nanotechnology* 18: 095702.
31. Chu S, Olmedo M, Yang Z, et al. (2008) Electrically pumped ultraviolet ZnO diode laser on Si. *Appl Phys Lett* 93: 181106.
32. Wang D, Reynolds N (2012) Photoluminescence of zinc oxide nanowires: the effect of surface band bending. *ISRN Condensed Matter Physics*.
33. Zhang Y, Gu S, Tang K, et al. (2015) Fabrication and characterization of highly oriented n-doped ZnO nanorods by selective area epitaxy. *J Nanomater.*
34. Yang HY, Lee SH, Kim TW (2010) Effect of $Zn(NO_3)_2$ concentration on the structural and optical properties nanostructures. *Appl Surf Sci* 256: 6117–6120.
35. Norberg NS, Gamelin DR (2005) Influence of the surface modification on the luminescence of colloidal nanocrystals. *J Phys Chem B* 109: 20810.
36. Qiu J, Li X, He W, et al. (2009) The growth mechanism and optical properties of ultralong ZnO. *Nanotechnology* 20: 155603.
37. Kwok WM, Djurišić AB, Leung YH, et al. (2005) Time-resolved photoluminescence study of the stimulated emission in ZnO nanoneedles. *Appl Phys Lett* 87: 09108.
38. Sun Y, Fuge GM, Fox NA, et al. (2005) Synthesis of aligned arrays of ultrathin ZnO nanotubes on Si wafer coated with a thin ZnO film. *Adv Mater* 17: 2477–2481.

39. Willander M, Yang LL, Wadeasa A, et al. (2009) Zinc Oxide nanowires: controlled low temperature growth and some electrochemical and optical nano-devices. *J Mater Chem* 19: 1006–1018.

AIMS Press